J. Synchrotron Rad. (2000). **7**, 368–373

Demonstration of X-ray linear dichroism imaging with hard X-rays

K. Sato,[a]* K. Okitsu,[a] Y. Ueji,[a] T. Matsushita[b] and Y. Amemiya[a,c]

[a]Department of Applied Physics, The University of Tokyo, Hongo, Bunkyo-ku, Tokyo 113-8656, Japan, [b]Institute of Materials Structure Science, High Energy Accelerator Research Organization (KEK), 1-1 Oho, Tsukuba, Ibaraki 305-0801, Japan, and [c]Department of Advanced Materials Science, The University of Tokyo, Hongo, Bunkyo-ku, Tokyo 113-8656, Japan. E-mail: sato@kohsai.t.u-tokyo.ac.jp

(*Received 9 May 2000; accepted 21 July 2000*)

X-ray polarization-contrast images resulting from X-ray linear dichroism (XLD) in the hard X-ray region have been successfully recorded for the first time. The apparatus used consisted of an X-ray polarizer, double X-ray phase retarders and a high-spatial-resolution X-ray charge-coupled device (CCD) detector. The sample used was a hexagonal close packed (h.c.p.) cobalt single-crystal foil of thickness about 12 μm. The experiment was performed at X-ray energies of 23 and 29 eV above the cobalt *K* edge (7709 eV), at which the maximum linear dichroisms (∼3%) were observed, with their signs reversed, in the XLD spectrum measured with quadruple X-ray phase retarders. The contrasts in the images at the two X-ray energies were reversed as a result of the XLD in the sample. Furthermore, the values of the contrast in the images arising from the linear dichroism (∼3%) were in good agreement with those yielded by the XLD spectrum.

Keywords: X-ray linear dichroism; polarization contrast; phase retarders; polarization switching; CCD detectors.

1. Introduction

Imaging of polarization contrast arising from X-ray dichroism has been attracting much attention with respect to investigations of magnetic, structural and chemical properties. Stöhr *et al.* (1993) have applied X-ray magnetic circular dichroism (XMCD) at the cobalt *L* edge (793, 778 eV) for the observation of magnetic domains of a magnetic recording disk, employing a photoelectron emission microscope (PEEM). Fischer *et al.* (1999) have used a transmission X-ray microscope (TXM) system composed of a Fresnel zone plate and a high-resolution CCD detector for XMCD imaging at the iron *L* edge (706 eV). Kagoshima *et al.* (1996) have used a scanning X-ray microscope (SXM) with a Fresnel zone plate for XMCD imaging at the nickel *L* edge (854 eV). Ade & Hsiao (1993) have obtained a polarization-contrast image resulting from X-ray linear dichroism (XLD) near the carbon *K* edge (285 eV), employing rotation of the specimen and a scanning transmission X-ray microscope (STXM). More recently, Stöhr *et al.* (1999) and Scholl *et al.* (2000) have observed images of antiferromagnetic structure by means of X-ray magnetic linear dichroism spectromicroscopy at the nickel *L* edge (∼870 eV) and at the iron *L* edge (∼720 eV), respectively. However, these imaging experiments have been restricted to the soft X-ray spectral range (less than 1 keV).

In the hard X-ray spectral range, above 1 keV, the first XLD spectrum was measured by Templeton & Templeton (1980) with samples rotated by 90° at the vanadium *K* edge (5.48 keV), using linearly polarized X-rays from synchrotron radiation. The XLD near an absorption edge originates from anisotropic environments around absorbing atoms. This method is called 'polarization XAFS' and has been used in some applications (Asakura *et al.*, 1999). However, this method cannot be extended to XLD imaging by the simple introduction of a high-resolution CCD detector because the sample used needs to be rotated by 90°, making it difficult to correct the non-uniformity of the sample thickness, as will be described in detail below.

By using a tunable X-ray polarimeter composed of a polarizer and an analyzer (Hart *et al.*, 1991), XLD spectra have also been obtained at the cobalt *K* edge (7709 eV). In that experiment, the XLD spectra were obtained *via* polarization ellipticity spectra of an X-ray beam transmitted by a cobalt crystal (Okitsu *et al.*, 1998). However, the X-ray throughput from the X-ray polarimeter was too low to record images with polarization contrasts arising from XLD.

The merits of XLD imaging with hard X-rays compared with soft X-rays are that the experiment can be performed under atmospheric conditions and that the large penetration depth could allow the observation of an inner three-dimensional polarization-sensitive structure of the mate-

rial, if tomography techniques are employed. In this paper, we will describe a method developed for the imaging of polarization contrast resulting from XLD in the hard X-ray spectral range. One of the key components of this method is a double X-ray phase retarder system (Okitsu *et al.*, 2000*a*), which compensates spherical aberration; alternatively, a quadruple X-ray phase retarder system can be employed (Okitsu *et al.*, 2000*b*), which compensates both spherical and chromatic aberrations. The use of either of these components represents an improvement over the conventional transmission-type phase retarder developed by Hirano *et al.* (1991, 1992, 1993, 1995). These aberration-compensating X-ray phase retarder systems in combination with a tunable X-ray polarizer, consisting of a Hart–Rodrigues type (Hart & Rodrigues, 1979) channel-cut silicon crystal, placed upstream, enable us to produce and switch high degrees of linear polarization between the horizontal and vertical directions. Another key component is a high-spatial-resolution CCD X-ray imaging system, composed of a CCD X-ray detector (Sato *et al.*, 2000).

The first observations of X-ray polarization-contrast images resulting from XLD in the hard X-ray spectral range are reported herein, for h.c.p. cobalt single crystals at the cobalt *K* edge (7709 eV).

2. Experiment

The experiments were performed at beamline BL-15B, at the Photon Factory (KEK). The experimental setup is represented schematically in Fig. 1. It consists of polarization-switching X-ray optics and a high-spatial-resolution X-ray CCD detector. In addition, the polarization-switching X-ray optics consists of a silicon 422 channel-cut offset X-ray polarizer and diamond 111 double phase retarders. The synchrotron white X-ray beam was monochromated and horizontally polarized in the vicinity of the cobalt *K* absorption edge (7709 eV) by the X-ray polarizer. The monochromated and horizontally polarized X-rays were incident on the double phase retarders. By adjusting the double phase retarders carefully, the polarization state of the transmitted X-rays can be switched between horizontal and vertical linear polarization with a high precision at a rate of 0.3 Hz. The degrees of horizontal and vertical linear polarization with this X-ray optical system were determined to be 99.99% and 95%, respectively. The X-ray intensity was reduced to 35% of the incident intensity by the introduction of the double phase retarders. Horizontally or vertically polarized X-rays transmitted by the sample were incident on the CCD detector. The CCD detector consists of a phosphor screen, a magnifying optical lens and a CCD. Gd_2O_2S:Tb (P-43) sedimented to a thickness of 6 μm on a beryllium plate was used as a phosphor screen. The magnification factor of the magnifying optical lens was fixed at ×10. The X-ray images were converted to visible-light images by the phosphor screen. The visible-light images were magnified by the magnifying optical lens and recorded on the CCD. The images were recorded with integration times of 60 min. The performance characteristics of this X-ray CCD detector system are presented in detail elsewhere (Sato *et al.*, 2000). The spatial resolution of this imaging system was evaluated to be 5.3 μm by a knife-edge technique.

The sample used was an h.c.p. cobalt single-crystal foil, of thickness 12 μm, the *c* axis of which, corresponding to an anisotropic axis, lay in the foil surface. Firstly, we measured the XLD spectrum of the sample in the vicinity of the cobalt *K* edge (7709 eV) by using the quadruple phase retarders. The degrees of horizontally and vertically linear polarization achieved with the quadruple phase retarder were 99.99% and 99%, respectively. The energy scan was performed by changing the Bragg reflection angle of the X-ray polarizer with an energy step of about 1.5 eV. Fig. 2 shows the XLD spectrum (solid line) together with the absorption spectrum (dashed line). It is seen that the measured XLD spectrum exhibits the largest negative and positive peaks (0.06 relative absorption difference) at photon energies of 23 and 29 eV, respectively, above the cobalt *K* edge (7709 eV) as a result of the XLD effect. Therefore, the X-ray energies were fixed at 23 and 29 eV above the cobalt *K* edge, at which the maximum polarization contrasts resulting from XLD are expected to be observed in the image.

Next, the sample was divided into three pieces, which were placed so that respective pieces were in the CCD field

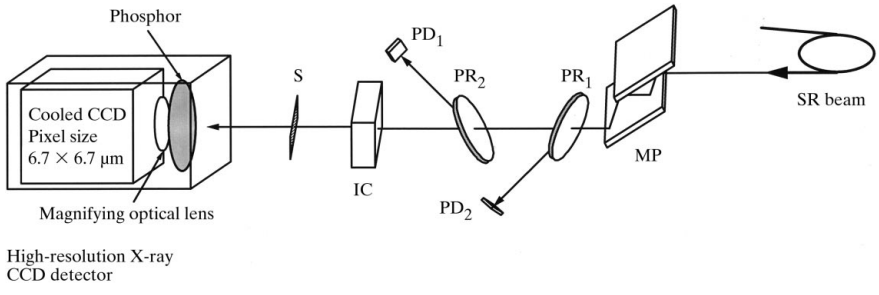

Figure 1
Experimental setup for acquiring images resulting from X-ray dichroism. MP: silicon 422 monochromating polarizer. PR_1 and PR_2: first and second diamond 111 phase retarders. PD_1: PIN photodiode monitoring X-rays reflected by the first phase retarder. PD_2: PIN photodiode monitoring X-rays Bragg-reflected by the second phase retarder. IC: ionization chamber monitoring X-rays incident to the sample. S: sample. SR: synchrotron radiation.

of view with their c axes inclined by 0, 90 and 45° from the horizontal plane, as shown in Fig. 3. We shall refer to these pieces as Area 1 (90°), Area 2 (0°) and Area 3 (45°). The CCD field of view is approximately 686 × 858 μm. After the backgrounds due to the dark current of the CCD detector were subtracted, the images were normalized according to integrated values determined by the ionization chamber (IC) placed upstream of the sample. Absorption images $(\mu t)_H(\mathbf{r})$ and $(\mu t)_V(\mathbf{r})$ were obtained from the normalized images recorded with and without the sample for horizontally and vertically polarized X-rays, respectively. We can assume that the polarization-independent absorption coefficient $(\bar{\mu})$ is equivalent to the average of two absorption coefficients for horizontally and vertically linear polarization (μ_H and μ_V),

$$\bar{\mu} = (\mu_H + \mu_V)/2. \quad (1)$$

Then the image of polarization-independent absorption may be written as

$$\bar{\mu}t(\mathbf{r}) = [(\mu t)_H(\mathbf{r}) + (\mu t)_V(\mathbf{r})]/2, \quad (2)$$

where $t(\mathbf{r})$ is the two-dimensional non-uniformity of the sample thickness. Thus, by using the value of $\bar{\mu}$ measured with the quadruple X-ray phase retarders, we can obtain $t(\mathbf{r})$ as follows,

$$t(\mathbf{r}) = (1/\bar{\mu})[(\mu t)_H(\mathbf{r}) + (\mu t)_V(\mathbf{r})]/2. \quad (3)$$

The images of the absorption coefficient for horizontally and vertically linear polarization [$\mu_H(\mathbf{r})$ and $\mu_V(\mathbf{r})$] are then written as

$$\mu_H(\mathbf{r}) = (\mu t)_H(\mathbf{r})/t(\mathbf{r}) \quad (4)$$

and

$$\mu_V(\mathbf{r}) = (\mu t)_V(\mathbf{r})/t(\mathbf{r}). \quad (5)$$

Hence, we can obtain the XLD image [XLD(**r**)] as follows,

$$\mathrm{XLD}(\mathbf{r}) = [\mu_V(\mathbf{r}) - \mu_H(\mathbf{r})]/[\mu_V(\mathbf{r}) + \mu_H(\mathbf{r})]. \quad (6)$$

Finally, a 10 × 10 binning was performed in order to reduce the fluctuation noise. The deterioration of the spatial resolution with this process is insignificant because the pixel size on the image (0.67 μm) is about one-tenth of the full width at half-maximum (FWHM) of the point spread function (PSF) (5.3 μm).

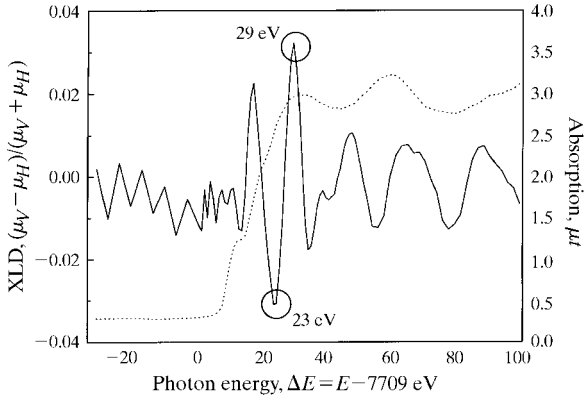

Figure 2
X-ray linear dichroism (XLD) spectrum (solid line) of an h.c.p. cobalt single crystal along with its absorption spectrum (dashed line), measured with the quadruple X-ray phase retarders.

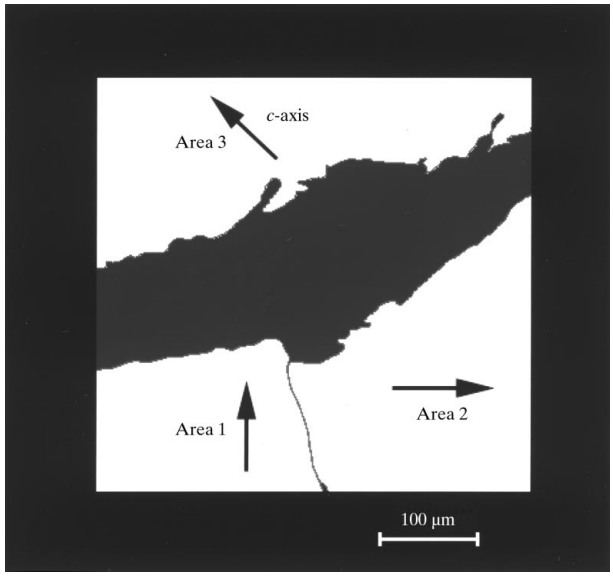

Figure 3
Arrangement of three pieces of the h.c.p. cobalt single crystal in the CCD field of view. The directions of the c axes are indicated by arrows.

3. Results and discussion

As discussed in the previous section, measured images have to be corrected against the non-uniformity of the sample thickness so that the images resulting from the polarization contrast can be extracted. Fig. 4 shows an image with contrasts arising from the non-uniformity of the sample thickness. The black part of the image represents an area of higher intensity, while the white part represents lower

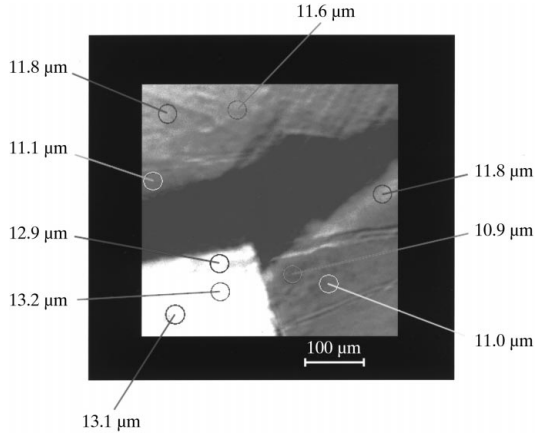

Figure 4
Image with contrasts arising from the non-uniformity of the sample thickness, at an X-ray energy of 7732 eV (23 eV above the cobalt K edge). Thicknesses are marked on the image.

intensity. The thicknesses at particular positions are indicated on the image.

Images with polarization contrasts arising from the XLD (Figs. 5*a* and 5*b*) were obtained at 23 and 29 eV above the cobalt *K* edge after correction of the contrast due to the non-uniformity of the sample thickness as shown in Fig. 4.

At a photon energy of 23 eV above the cobalt *K* edge, Area 1, Area 2 and Area 3 appear white, black and grey, respectively (Fig. 5*a*). This means that the X-ray intensities are the highest in Area 1 and the lowest in Area 2. In order to extract further information, we have calculated the values of the XLD from the averaged pixel values in the respective areas. The calculated values of the XLD in Area 1, Area 2 and Area 3 are 0.027, −0.023 and −0.013, respectively, as shown in Fig. 5(*a*). These values approximately agree with those of the XLD spectrum measured with the quadruple X-ray phase retarders. However, strictly speaking, there exist slight differences in the values of XLD between the images and the spectrum. A discussion of these slight differences is presented in the following paragraph. At a photon energy of 29 eV above the cobalt *K* edge, the contrasts in the image were reversed in Area 1 and Area 2, whereas the contrast in Area 3 remained the same. The values of the XLD in Area 1, Area 2 and Area 3 are −0.020, 0.024 and −0.010, respectively, as shown in Fig. 5(*b*); these values are approximately in agreement with those of the XLD spectrum. Hence it is concluded that these contrasts originate from the orientation of the *c* axis, that is, genuinely originating from the XLD of the h.c.p. cobalt single crystals.

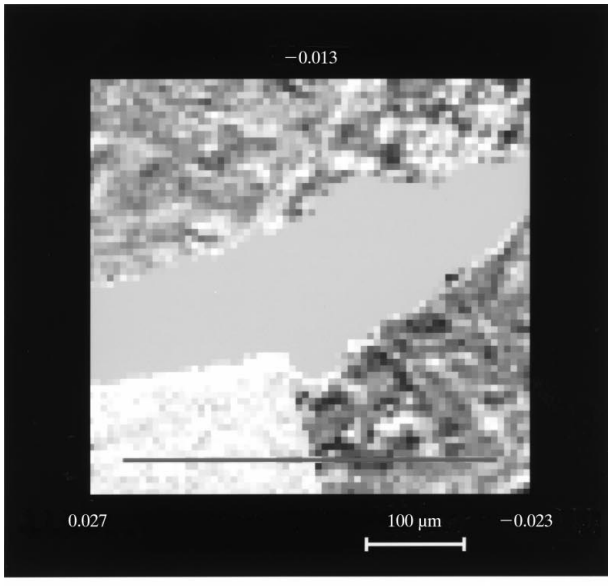

(*a*)

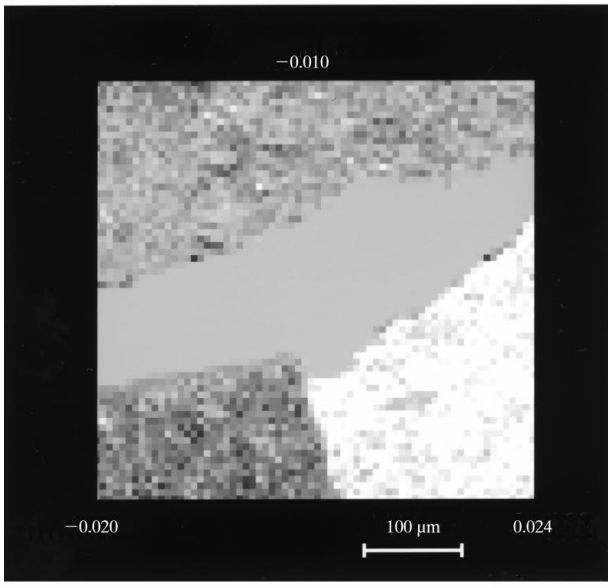

(*b*)

Figure 5
Images resulting from X-ray linear dichroism (XLD) taken at (*a*) 23 eV and (*b*) 29 eV above the cobalt *K* edge after correction for non-uniformity of the sample thickness.

In this paragraph, we discuss the slight differences between the values of the XLD obtained from the images and those from the XLD spectrum. As already mentioned, the XLD spectrum seen in Fig. 2 was measured using the quadruple X-ray retarders composed of four successive transmission-type diamond crystals, by which both spherical and chromatic aberrations are compensated. This optical system yields a higher degree of linear polarization (99%) in the vertical direction than the double phase retarders (95%). Nevertheless, we performed the XLD imaging with the double phase retarders in order to obtain higher X-ray intensities. Hence, the slight differences are attributed to the differences of the degree of linear polarization in the vertical direction.

Next, we discuss the statistical fluctuation observed in the XLD images shown in Fig. 5. The one-dimensional profile of the XLD along the line in Fig. 5(*a*) is shown in Fig. 6. The fluctuation of the XLD value in an area can be attributed to statistical fluctuations originating from both photon statistics and the readout noise of the CCD. Figs. 6(*a*) and 6(*c*) show the profiles before and after the 10×10 binning, respectively. The fluctuation derived from photon statistics ($\sigma_{\rm xph}$) and the readout noise ($\sigma_{\rm readout}$) of the CCD propagate according to the law of error propagation in the calculation process described in the previous section. Then, the fluctuation of the XLD value ($\sigma_{\rm XLD}$) can be calculated from the equation

$$\sigma_{\rm XLD} = (\sigma_{\rm xph}^2 + \sigma_{\rm readout}^2)^{1/2}. \qquad (7)$$

$\sigma_{\rm readout}$ amounts to 4.3×10^{-2}, according to the calculation based on the readout noise (∼5 electrons r.m.s.) of the CCD and the ADC gain (0.06 electrons/ADC), whereas $\sigma_{\rm xph}$ amounts to $\sim 2.1 \times 10^{-1}$, based on the conversion gain (0.34 electrons/xph). Then, $\sigma_{\rm xph}$ seems to be dominant in the value of $\sigma_{\rm XLD}$. However, when the spatial resolution of the CCD (∼5.3 μm in FWHM) is taken into account in relation to the CCD pixel size on the image (0.67×0.67 μm), $\sigma_{\rm xph}$ is expected to be reduced to one-tenth because of the cross talk (*i.e.* blurring) between neighbouring pixels. Therefore, the resultant $\sigma_{\rm xph}$ is expected to

be $\sim 2.1 \times 10^{-2}$. This explains the fluctuation of the XLD shown in Fig. 6(*a*), which amounts to $\sim 5 \times 10^{-2}$.

The fluctuation of the XLD in Fig. 6(*a*) was reduced with a 1×10 binning, as shown in Fig. 6(*b*). With the 10×10 binning, the fluctuation of the XLD was further reduced to 5×10^{-3}, which corresponds to one-tenth of that before the binning. The deterioration in the spatial resolution is negligible with the 10×10 binning because the FWHM of the PSF of the X-ray CCD detector ($\sim$5 μm) is about ten times as large as that of the CCD pixel size on the image (0.67 μm). A low-frequency component of the fluctuation observed in the XLD profile of Fig. 6(*c*) is considered to be a residual of the correction of the sample thickness.

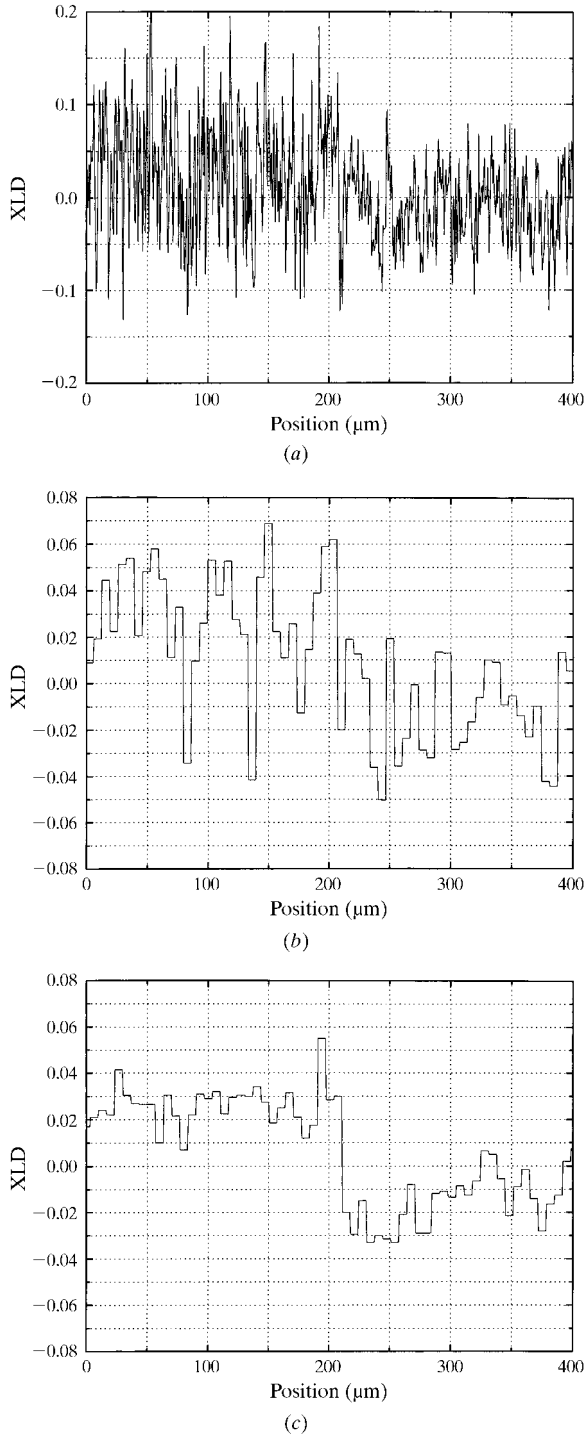

Figure 6
X-ray linear dichroism (XLD) profiles along the line in Fig. 5(*a*): (*a*) without binning, (*b*) with a 1×10 binning, and (*c*) with a 10×10 binning.

Finally, we discuss the merits of using the polarization-switching optics compared with the method of rotation of the sample. As described above, the raw image data were dominated by the effect of non-uniformity of the sample thickness. Therefore, it is critical to correct the thickness effect precisely so that only the polarization effect, which is much smaller than the thickness effect, is correctly extracted. When we choose to rotate the sample, there are two possibilities as to whether or not the X-ray CCD detector is rotated together with the sample. If the X-ray CCD detector is not rotated, both non-uniformities of the response of the X-ray CCD detector ($\sim$13%) and of the incident X-ray beam intensity prohibit the precise correction of the sample thickness effect. When the X-ray CCD detector is rotated with the sample, there still remains the effect of non-uniformity in intensity of the incident X-ray beam, which also deteriorates the correction of the sample thickness effect. Accordingly, it is difficult to extract the polarization contrast from the raw images with rotation of the sample. On the contrary, when the direction of the polarization of the incident X-ray beam is switched, neither the non-uniformity of the response of the X-ray CCD detector nor that of the intensity of the incident X-ray beam affect the correction of the sample thickness effects. This advantage could justify the cost in intensity ($\sim$64%) due to the introduction of the double phase retarders.

In this study, we have placed emphasis on the observation of the polarization-contrast image resulting from XLD in the hard X-ray region, putting aside the spatial resolution. However, it should be noted that the microimaging of polarization contrast ($\sim$3%) with a spatial resolution of 5 μm is also possible with the apparatus.

4. Conclusions

We have developed a method to obtain microimages resulting from X-ray linear dichroism (XLD) by combining polarization-switching X-ray optics with a high-spatial-resolution X-ray CCD detector. With this method, XLD images with about 3% contrast at the cobalt *K* edge (7709 eV) have been clearly obtained for h.c.p. cobalt single crystals displaying anisotropy of absorption and artificially prepared so that the *c* axes of the crystals were orientated in three different directions (0, 90 and 45°). In addition, this method can be applied to studies of the domain structures of polycrystalline material. It can also be applied to microimaging of magnetic linear dichroism (XMLD) and magnetic circular dichroism (XMCD) at the *K* edges of transition metals and the *L* edges of rare-earth elements.

The authors would like to thank Dr Y. Hasegawa, Atominstitut der Osterreichischen Universiten, for valuable discussions. This work is supported by a Grant-in-Aid for COE Research and a Grant-in-Aid for Scientific Research (B) of the Ministry of Education, Science, Sports and Culture. This work was performed under the approval of the Photon Factory Program Advisory Committee (Proposal No. 97G-075).

References

Ade, H. & Hsiao, B. (1993). *Science*, **262**, 1427–1429.

Asakura, K., Kubota, T., Chun, W. J., Iwasawa, Y., Ohtani, K. & Fujikawa, T. (1999). *J. Synchrotron Rad.* **6**, 439–441.

Fischer, P., Schütz, G., Schmahl, G., Guttmann, P. & Raasch, D. (1999). *Z. Phys. B*, **101**, 313–316.

Hart, M. & Rodrigues, A. R. D. (1979). *Philos. Mag. B*, **40**, 149–157.

Hart, M., Siddons, D. P., Amemiya, Y. & Stojanoff, V. (1991). *Rev. Sci. Instrum.* **66**, 2540–2544.

Hirano, K., Ishikawa, T. & Kikuta, S. (1993). *Nucl. Instrum. Methods. A*, **336**, 343–353.

Hirano, K., Ishikawa, T. & Kikuta, S. (1995). *Rev. Sci. Instrum.* **66**, 1604–1609.

Hirano, K., Ishikawa, T., Koreeda, S., Fuchigami, K., Kanzaki, K. & Kikuta, S. (1992). *Jpn J. Appl. Phys.* **31**, L1209–L1211.

Hirano, K., Izumi, K., Ishikawa, T., Annaka, S. & Kikuta, S. (1991). *Jpn J. Appl. Phys.* **30**, L407–L410.

Kagoshima, Y., Miura, T., Ando, M., Wang, J. & Aoki, S. (1996). *J. Appl. Phys.* **80**, 3124–3126.

Okitsu, K., Oguchi, T., Maruyama, H. & Amemiya, Y. (1998). *J. Synchrotron Rad.* **5**, 995–997.

Okitsu, K., Ueji, Y., Sato, K. & Amemiya, Y. (2000*a*). *J. Synchrotron Rad.* Submitted.

Okitsu, K., Ueji, Y., Sato, K. & Amemiya, Y. (2000*b*). In preparation.

Sato, K., Hasegawa, Y., Kondo, K., Miyazaki, K., Matsushita, T. & Amemiya, Y. (2000). *Rev. Sci. Instrum.* Accepted.

Scholl, A., Stöhr, J., Lüning, J., Seo, J. W., Fompeyrine, J., Siegwart, H., Locquet, J.-P., Nolting, F., Anders, S., Fullerton, E. E., Scheinfein, M. R. & Padmore, H. A. (2000). *Science*, **287**, 1014–1016.

Stöhr, J., Scholl, A., Regan, T. J., Anders, S., Lüning, J., Scheinfein, M. R., Padmore, H. A. & White, R. L. (1999). *Phys. Rev. Lett.* **83**, 1862–1865.

Stöhr, J., Wu, Y., Hermsmeier, B. D., Samant, M. G., Harp, G. R., Koranda, S., Dunham, D. & Tonner, B. P. (1993). *Science*, **259**, 658–661.

Templeton, D. H. & Templeton, L. K. (1980). *Acta Cryst.* A**36**, 237–241.